High-strength bacterial cellulose-polyacrylamide hydrogels: Mesostructure anisotropy as studied by spin-echo small-angle neutron scattering and cryo-SEM

Velichko, Evgenii; Buyanov, A.L.; Saprykina, N.N.; Chetverikov, Yu.O.; Duif, Chris; Bouwman, Wim; Smyslov, R.Yu.

Important note
To cite this publication, please use the final published version (if applicable).
Please check the document version above.

High-Strength bacterial cellulose–polyacrylamide hydrogels: mesostructure anisotropy as studied by spin-echo small-angle neutron scattering and cryo-SEM

Velichko E.V.[1,2], Buyanov A.L.[3](✉), Saprykina N.N. [3], Chetverikov Yu.O.[2], Duif C.P.[1], Bouwman W.G. [1], Smyslov R.Yu.[2,3]

[1] *Delft University of Technology, Delft, The Netherlands*

[2] *Petersburg Nuclear Physics Institute, National Research Center "Kurchatov Institute", Gatchina, Leningrad district, Russia.*

[3] *Institute of Macromolecular Compounds, Russian Academy of Sciences, Saint Petersburg, Russia*

Velichko Evgenii V.

Delft University of Technology, Mekelweg 15, 2629JB Delft, The Netherlands; Ph.: +31-(0)15 27 85731, Fax:+31-(0)15 27 88303, E-mail: e.velichko@tudelft.nl Petersburg Nuclear Physics Institute, National Research Center "Kurchatov Institute", OrlovaRoscha, Gatchina, Leningrad district, 188300, Russia; Ph.: +7(813-71) 46025, Fax: +7(813-71) 36025, E-mail: evgen.velichko@lns.pnpi.spb.ru

Buyanov Alexander L.

Institute of Macromolecular Compounds, Russian Academy of Sciences, Saint Petersburg, Bolshoy pr., 31, Saint Petersburg, 199004, Russia;

Ph.: +7(812)328-6879,

Fax: +7(812)328-6869,

E-mail: buyanov799@gmail.com

Chetverikov Yurii O.

Petersburg Nuclear Physics Institute, National Research Center "Kurchatov Institute", OrlovaRoscha, Gatchina, Leningrad district, 188300, Russia; Ph.: +7(813-71) 46025, Fax: +7(813-71) 36025, E-mail: yurka@lns.pnpi.spb.ru

Duif Chris P.

Delft University of Tehchnology, Mekelweg 15, 2629JB Delft, The Netherlands; Ph.: +31-(0)15 27 84267, Fax:+31-(0)15 27 88303, E-mail: c.p.duif@tudelft.nl

BouwmanWim G.

Delft University of Tehchnology, Mekelweg 15, 2629JB Delft, The Netherlands; Ph.: +31-(0)15 27 84267, Fax:+31-(0)15 27 88303, E-mail: w.g.bouwman@tudelft.nl

Smyslov Ruslan Yu.

Institute of Macromolecular Compounds, Russian Academy of Sciences, Saint Petersburg, Bolshoypr-t, 31, Saint Petersburg, 199004, Russia; Ph.: +7(812)328-8538, Fax: +7(812)328-6869, E-mail: urs@mail.macro.ru

Petersburg Nuclear Physics Institute, National Research Center "Kurchatov Institute", OrlovaRoscha, Gatchina, Leningrad district, 188300, Russia; Ph.: +7(813-71) 46025, Fax: +7(813-71) 36025, E-mail: urs@mail.macro.ru

Abstract. Submicron- and micron-scale structures of composite hydrogels based on bacterial cellulose (BC) and polyacrylamide were studied by spin-echo small-angle neutron scattering (SESANS) and cryo-scanning electron microscopy (cryo-SEM). These hydrogels possessing the structure of interpenetrating polymer network were synthesized via free-radical polymerization of acrylamide carried out in the pellicle of BC swollen in the reaction solution. No neutron scattering was observed for the samples swollen in heavy water to the equilibrium state, but the SESANS signal appeared when TbCl$_3$ salt was added to the solvent. It is the unusual effect, which may be very helpful for SESANS studying of other hydrogel systems. The SESANS dependences obtained for these samples revealed the anisotropy of mesostructure for the hydrogels under investigation. Density inhomogeneities on the characteristic scale of 11.5 ± 0.5 µm were detected in one fixed orientation of the sample, i.e. with the growth plane of BC parallel to the plane formed by the neutron beam and the spin-echo length. The uniaxial anisotropy revealed agrees with a recently proposed model, which attributes this behavior to the existence of tunnel-like oriented structures inside BC. The evidence of such type of mesostructure anisotropy of BC and BC-PAAM hydrogels was obtained by using the cryo-SEM method.

Keywords SESANS, SEM, interpenetrating polymer network, hydrogel, bacterial cellulose, polyacrylamide, terbium, luminescence, anisotropy, polymeric composite

Abbreviations
BC: bacterial cellulose;
Cryo-SEM: cryo scanning electron microscopy
IPNs: interpenetrating polymeric networks;
PAA: polyacrylic acid;
PAAm: polyacrylamide;
PVA: polyvinyl alcohol
SANS: small angle neutron scattering
SESANS: spin-echo small-angle neutron scattering;
SLD: scattering length density.

Introduction

Hydrogels are three-dimensional crosslinked structures formed by hydrophilic polymers. One of the promising fields of hydrogels' application is the development of biomaterials (implants for medical use). For example, hydrogels based on PVA are already being used as artificial cartilages to substitute the injured natural ones [1, 2]. Currently, however, the problem of improving the mechanical properties of these hydrogels and reaching characteristics of natural articular cartilage has not been completely solved [3], and this situation hampers wider use of hydrogels in medicine. The high level of the hydrogel's mechanical characteristics is also necessary for the developments of various type of chemo-mechanical systems, hydrogel actuators, and so on [4].

In recent years, cellulose and its distinctive type, namely BC, have been used for the synthesis of various types of advanced composite materials including hydrogel compositions for biomedical applications [5—7].

One well-known method of designing composite materials with improved functional properties is the synthesis of compositions possessing the structure of interpenetrating polymer networks [8]. We have used this method to develop the hydrogel consisting of cellulose—polyacrylamide and cellulose—polyacrylic acid compounds [9–12]. Due to the high rigidity of cellulose chains, these hydrogels possess high mechanical strength and stiffness, and at the same time retain all valuable properties inherent to PAAm and PAA. These hydrogels exhibit high stiffness, strength, and flexibility under different types of mechanical loads,

including long-acting cyclic compression load [11, 12]. In the synthesis of our hydrogels, we used bacterial or plant cellulose as a reinforcing component.

Buyanov et al. [11] have for the first time observed an important feature of the BC-PAAm hydrogel, i.e., an anisotropy of mechanical properties, which is detected during compression. All mechanical characteristics of these materials are considerably higher when measured along the direction perpendicular to the growth surface of the original BC matrix. The authors suggested that the anisotropy of mechanical properties of BC-PAAm hydrogels is associated with structural features of BC. According to Thompson et al. [13], BC has "tunnels" oriented mainly in the vertical direction; bacteria form these tunnels during biosynthesis. "Walls" of such tunnels can be condensed by congestions of the rigid chain microfibrillar BC ribbons, and these ribbons are able to reinforce mechanically hydrogels under compression in the vertical direction. In our case, tunnel lacunas in the BC structure are filled with relatively soft polyacrylamide chains, this resulting in lower compressive stiffness in the direction along the surface of the BC [11]. It should be noted that the anisotropic mechanical behavior observed experimentally could be also assigned to the existence of other types of ordering in the BC structure.

Recently [14a], SANS has been applied to characterize the structure of pure bacterial cellulose hydrogels, and composites thereof, with two plant cell wall polysaccharides (arabinoxylan and xyloglucan). The authors developed a suitable theoretical model to describe the scattering arising from hierarchically assembled pure bacterial cellulose, and its composite hydrogels with two different plant cell wall polysaccharides.

In our study [14b], we propose to use Tb^{3+} to obtain contrast at studying the mesostructure of one type of BC-PAAm hydrogels by spin-echo small angle neutron scattering (**SESANS**). Following Håkansson [14c], salt addition might also change the mechanical properties of cellulose but this assumption ought to be approved in our case still. We use the complementary cryo-SEM method to explain structural heterogeneities and the ordered and oriented regions. Existence of these regions is expected to lead to the observed anisotropy of mechanical characteristics. As follows from [13], the size of oriented regions in the BC structure can reach several micrometers. The use of SESANS provides information on the structural inhomogeneities with a size up to 18 or more micrometer [15], whereas the classical SANS is designed to study inhomogeneities less than a micrometer in size. SANS was previously applied to identify inhomogeneities as large as 100 nm in PAAm and PAA hydrogels [16].

Materials

Synthesis of BC

BC was grown by using the *Gluconacetobacter xylinus* strain (№1629 CALU) of St. Petersburg's State University (the department of microbiology) in water solutions containing 2 wt.% of glucose, 0.3 wt.% of yeast extract and 2 wt.% of ethanol at 30°C for 14 days in cylindrical glass vessels, as described in detail in [11]. The BC was subsequently washed in water solutions of potassium hydroxide at 100°C and then washed in water at room temperature. The resulting BC samples were gel-like pellicles with a thickness up to 25 mm, containing approx. 99 wt. % of water. In Fig. 1a we demonstrate the native BC until the reaction of

Synthesis of composite BC—PAAm hydrogels

Samples of BC—PAAm hydrogels were prepared using our formerly developed technique of synthesis of composite hydrogel materials [9—12]. Acrylamide (Aldrich Chemicals) was recrystallized twice from benzene. All other reagents of analytical grade were used as received. The hydrogels were synthesized by immersing matrices containing about 1 wt. % of BC into a large amount of aqueous reaction solutions containing 55 wt. % of acrylamide for 16 hrs. N,N'methylenebisacrylamide was used as the crosslinking agent at a concentration of 1.4×10^{-3} M. Freeradical polymerization was initiated by cobalt (III) acetate (at a concentration of 1×10^{-3} M); the process was conducted in cylindrical glass vessels as large as 8 cm in diameter [11]. When the synthesis was completed, the composite hydrogels in the form of a round flat layer obtained in varying thicknesses up to 3 cm were placed in distilled water for several days to remove low molecular weight components and to let the gels swell. The cutting of composite hydrogel is shown in Fig. 1b.
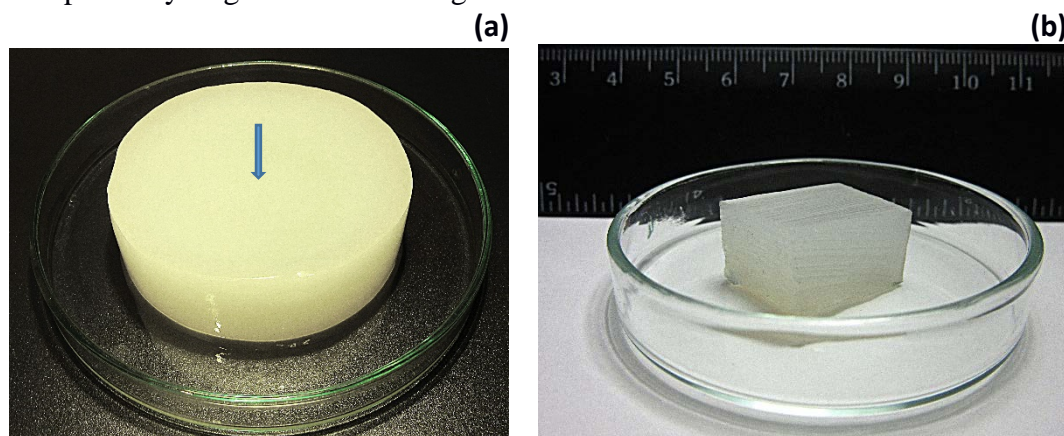

Fig. 1. The photograph of native BC (a) and synthesized composite hydrogel based on it (b). The initial surface of BC growth is indicated by a blue arrow.

Equilibrium water content in hydrogels was determined gravimetrically by weighing the swollen samples and the same samples dried until constant weight was reached (at 160°C). The content of BC in BC-PAAm composition (as defined by known concentrations of BC and monomer in the reaction solution) was equal to 2 wt. % (the monomer conversion in the synthesis conditions was close to 100% [11]). The equilibrium water content in hydrogel samples was 70±3 wt. %.

Preparation of samples for SESANS

For SESANS experiments, rectangular blocks of $l \times w \times h$ sizes equal to $10 \times 9 \times 5$ mm (HG1), or $16 \times 10 \times 5$ mm (HG2) were cut out from the round flat layer of synthesized hydrogels (Table 1). To obtain luminescent hydrogels, which are available for investigating by neutron methods with contrasting original materials, the sorption of terbium chloride (III) solution was carried out in D_2O by a hydrogel.

99.9% terbium chloride (III) hexahydrate ($TbCl_3 \cdot 6H_2O$) of reagent grade (CAS 13798-24-8) was purchased from Sigma-Aldrich and used without further purification to prepare aqueous (D_2O) solutions of two concentrations: 0.36 and

4

1.42 mg /mL for HG1Tb and HG2Tb, respectively (see Table 1). Sorption of Tb^{3+} ions was implemented the following way: The initial block of a hydrogel (HG1 or HG2) containing H_2O was first dried at 54°C until constant weight was reached. It was then placed in the 10-fold (by volume) excess of the D_2O solution of terbium chloride (III) to attain equilibrium swelling at ambient temperature. It follows that the hydrogel block was as full of the $TbCl_3$ solution in "heavy" water as possible instead of "light" water.

Table 1. Hydrogels based on BC and PAAm: concentration of salt solution in D_2O used for swelling (c_{TbCl3}), the geometry of hydrogel block after swelling

№	Sample	c_{TbCl3}, mg/mL	$l \times w \times h$, mm^3
1	HG	0	16×10×5
2	HG1Tb	0.36	16×10×5
3	HG2Tb	1.42	10×9×5

Methods

SESANS

The structure of the hydrogels was studied by SESANS. The measurements were carried out at the SESANS Delft setup (RID research reactor at the Delft University of Technology, The Netherlands) [17]. The SESANS setup has the following characteristics: wavelength λ = 2.09 Å, $\Delta\lambda/\lambda$ = 2%, range of measured spin-echo lengths z = 0.030 — 18 μm, the initial polarization of the incident beam P = 0.93, the sample-detector distance is fixed at 3658 mm.

The entire available range of spin-echo lengths (values of z) was employed in the measurements. The polarization of the transmitted beam after the sample for each value of z was normalized to the one of the beam transmitted through 99% D_2O to take into account the effect of the solvent, equipment characteristics, cuvettes, and background in the scattering pattern. All measurements were carried out at room temperature and atmospheric pressure. The samples consisted of rectangular blocks (Table 1) placed in quartz cuvettes with dimensions of 5 × 10 × 50 mm. Each block of hydrogel with $l \times w \times h$ dimensions was measured in three orientations relative to the setup axes z and k, where z is the spin-echo length, and k is the direction of the neutron beam (Fig. 2a). Attention was paid to the orientation of the BC growth surface of synthesized HG blocks. It corresponds to the plane (l × w), which is highlighted by the grid pattern in Fig. 2a.

In neutron experiments, scattering occurs due to a contrast in the neutron scattering length densities; in the two-phase system approach, the contrast is described by the formula:

$$\Delta\rho = |\rho_1 - \rho_2|, \qquad (1)$$

where ρ_1 and ρ_2 are the SLDs of the first and second phases forming the object under study, respectively. The SLD, in turn, was calculated by the formula:

$$\rho = N\sum_i b_i = (\delta N_A/M)\sum_i b_i, \qquad (2)$$

where δ is the volume density of the object, N is the volume concentration of scattering centers, M is the relative molecular mass, N_A is the Avogadro's number, b_i is the scattering length of the ith nucleus in the molecule. The length densities of

coherent scattering ρ_{coh} for the phases that constituted the objects under investigation are listed in Table 2. When calculating the contrasts, two situations were considered: (*i*) homogeneous distribution of $TbCl_3$ salt between phases (then, the mass percentage in HG1Tb would be 0.024% and in HG2Tb it would be 0.105%); (*ii*) selective sorption of terbium ions on BC microfibrils, then the *maximum* mass content of HG2Tb(sel) would be 1.09% assuming full absorption of terbium ions by the hydrogel from the solution.

Table 2. Scattering length densities and phase volume fractions φ_n of the kth component in the HG, HG1Tb and HG2Tb at the equal sorption of $TbCl_3$ and in HG2Tb(sel) and the selective sorption

№	Hydrogel component	Formula	$\delta^{1)}$, g/cm^3	ρ_{coh} (10^{14}/m^2)	φ_k, vol.% in hydrogel			
					HG	HG1Tb	HG2Tb	HG2Tb (sel)
1	Acrylamide unit	(-CH$_2$CHCONH$_2$-)$_n$	1.34	1.81	28.7	28.7	22.1	22.0
2	Cellulose unit	(-C$_6$H$_{10}$O$_5$-)$_n$	1.5	1.76	0.523	0.523	0.402	0.401
3	Terbium chloride	TbCl$_3$	4.35	3.56	0	$6.41 \cdot 10^{-3}$	0.0281	n/a$^{2)}$
4	Hexohydrate terbium chloride	TbCl$_3$ x 6(H$_2$O)	4.35	1.83	n/a	n/a	n/a	0.411
5	Heavy water	D$_2$O	1.11	6.34	70.8	70.8	77.5	77.2

Note:
[1] the density component used in the calculation of the ρ_{coh} value;
[2] n/a – not applicable.

So, physico-chemical characteristics of components of the hydrogels and the volume fraction attributed to each phase are shown in Table 2.

The value of transmission T for hydrogels measured versus the cuvette with D$_2$O was *ca*. 0.7. The observed decrease of T for hydrogels by ~ 30% compared to that of D$_2$O can be explained by two factors. First, the sample can contain scattering inhomogeneities, which are smaller than the setup resolution (< 0.030 µm). The scattering occurs at wide angles (it is known that $\theta \propto 1/d$, where θ is the scattering angle, and d is the intrinsic dimension of the scattering particles), and, as a result, the scattered neutrons do not fall within the aperture before the detector. Secondly, the samples contain hydrogen atoms, and this fact leads to considerable incoherent scattering. The latter also causes the output of scattered neutrons outside the detector aperture. It is revealed that the values of T for all samples are close to each other; therefore, we draw a conclusion that the above two parameters (the presence of small-scale inhomogeneities and presence of incoherently scattering centers) are inherent to all samples.

In the SESANS experiment, one measures the polarization of the neutron beam as a function of spin-echo length (the distance in real space). For each spin-echo length, two measurements of the polarization are carried out after passing through both the sample, and the setup at the same conditions, but without the sample (empty beam measurement). Then, the beam polarization after the sample is normalized to the polarization of the beam passing through the cuvette with D$_2$O. The SESANS data processing was carried out using cylindrical model (see Appendix A) [15, 18—19].

6

Photoluminescence spectra

Photoluminescence emission and excitation spectra for BC—PAAm hydrogels containing Tb^{3+} ions were registered using the LS-100 BASE luminescence spectrophotometer (*PTI Lasers INC*, Canada). When using a holder for solid samples, the luminescence intensity I_{lum} was recorded from the side of incidence of the exciting light beam. In the phosphorescence mode, the used integration window recorded the intensity I_{lum} between 100 and 2000 μs. The <mark>grazing-incidence</mark> angle for the excitation light beam with respect to the sample was ~30°. Wavelength range for emission spectra was 460—700 nm at excitation wavelength λ_{exc} = 299 nm; for excitation spectra it was 210—400 nm at the wavelength of luminescence observation λ_{em}=543 nm. The spectral width of monochromator slits for the excitation and luminescence was 4 nm; the PMT gain was500.The values of I_{lum} for correct comparison were reduced to an internal laboratory standard.

Cryo-SEM

Cryo-SEM was performed on a Supra 55VP scanning electron microscope (Zeiss, Germany) equipped with a PP 2000T Cryo-SEM system (Quorum Technologies, the United Kingdom). The BC containing ~99 wt. % of water and hydrogel sample swollen to the equilibrium state were rapidly frozen in liquid nitrogen and then transferred to preparation chamber cold stage (-140 °C) and fractured. The sample chips were made so that their surface focused mainly perpendicular to the surface of growth of matrix BC. For improving contrast, the sample surface was coated with platinum by cathode sputtering. For ice sublimation, etching of the surface and revealing structure, temperature of the cold stage was raised to −90°°C. After coating with platinum, the sample transferred to the cold SEM stage (-140 °C). Independent cooling the cold stage and the cold trap (-190 °C) prevented ice buildup on the sample. The surface morphology was studied using the secondary electron mode (SE2).

Results and Discussion

For SESANS experiments, we have chosen one of the most interesting BC—PAAm hydrogels for practical use, which recently successfully passed the preliminary tests as artificial cartilage during *in vivo* experiments conducted on rabbits [20]. As tentative experiments showed, the measurements of the samples swollen in heavy water are not informative (no spin-echo depolarization), we have tested the option of introducing terbium ions into hydrogels by swelling the samples in a solution of $TbCl_3$ at two concentrations: 0.36 and 1.42 mg/mL for HG1Tb and HG2Tb, respectively (Table 1).

It is further known that the metal ions are capable of selective adsorption on cellulose fibrils [21, 22]. Therefore, it is possible to assume that the sorption of terbium ions on a polymeric matrix permits a depolarization to be sufficient, especially, if this sorption might preferably occur on cellulose. The microfibrillar structure of bacterial cellulose is well-studied [23]: It is formed by swollen microfibrillar ribbons (ca. 70—145 nm wide) consisting of 5 to 12 water-free I_{α}-crystalline subunits with a cross-section of about 7 nm x 13 nm and of water solvating the subunits. At that, lateral aggregation of these crystalline units was

found along the smaller (110)-lattice planes with a layer of water between adjacent crystallites [23]. This structure of BC can quite promote its high ability to strongly coordinated binding of metal ions, such as Tb^{3+}. This consideration especially holds true if it is taken according to Fink's model that there is, however, a small amount of noncrystalline tie-molecules arising from surface distortions, which connect the crystalline units laterally.

In this regard, we can consider the phase consisting of {$BC+TbCl_3\times6H_2O$}. Possibly, terbium ions contain aqua ligands and bound "light" water in their coordination spheres; this water can remain after the cyclic drying. Then the mass content of $TbCl_3$ salt in the hydrogel is 1.09%, i.e. an order of magnitude higher than that in the case of non-selective sorption. The volume portion of salt hydrate can reach 0.411%; this value is comparable to the portion of BC (Table 2, compare the rows 2 and 4 for the HG2Tb(sel) column).

In order to unveil the mesostructural anisotropy, all the samples were measured with SESANS in three different orientations (Fig. 2a). The dependences of the reduced polarization P (z) on the spin-echo length z for three orientations of HG2Tb (Fig. 2b, curves *1—3*) are shown in Fig. 2b, curves *1—3*). For orientations 1 and 3 (see curves *1* and *3*), the amplitude of the spin-echo polarization is close to unity throughout the entire z range studied, we can assume, therefore, absence of the inhomogeneities on this length scale. For orientation 2, a decay in $P(z)$ is observed from 1.00 to 0.68 with further levelling-out at z values higher than 12 μm.

For the HG1Tb, shapes of dependences in the orientations 1 and 3 are not shown in Fig. 2b, because they coincide with the behavior of the dependence obtained for HG2Tb. The HG1Tb also demonstrates the presence of heterogeneities only in orientation 2; at the same time, the difference between the amplitudes of the spin echo signal at small and large z values (> 11 μm) is much smaller (1 to 0.9) than that for the HG2Tb sample (see curve 2', Fig. 3b). For the HG sample in all three orientations, the spin-echo signal is equal to unity throughout the whole range of spin-echo lengths, which might indicate the absence of scattering inhomogeneities on the length-scales studied.

The decrease in the amplitude of the spin-echo signal for the HG1Tb and HG2Tb samples is caused by the presence of inhomogeneities of the size lying within the z-range studied. The presence of contrast in only one of three orientations indicates a uniaxial anisotropy of the structure of the PAA–BC complexes. This anisotropy can be inherited only from the BC, which is a rigid scaffold of the entire multiphase system. The heterogeneity was observed in the direction parallel to the surface of the BC growth. It means that the observed inhomogeneities are focused mainly in the direction perpendicular to the growth surface of the original BC matrix.

The fact that contrast was detected only in the systems containing $TbCl_3$ may be explained by both selective sorption of Tb^{+3} ions on the BC microfibril surface, and by the spatial separation of PAA/BC/D_2O phases in the alkaline $TbCl_3$-containing solution. We suppose that because of the negative ζ-potential of BC [24] and the complex ability of Tb^{3+} [25], this ions preferably condense on microfibrils of BC, i.e. they contrast mostly the so-called "tunnel" walls (Fig. 4 and 5). For comparison, the analogy to obtain a contrast for the SESANS investigation of composite hydrogel mesostructure using counterions could be made with the study of the rod-like polyelectrolytes in aqueous solutions surrounded by counterions by anomalous small angle X-ray scattering (ASAXS) [26a]. Furthermore, trivalent counterions are localized around macroions more

8

345
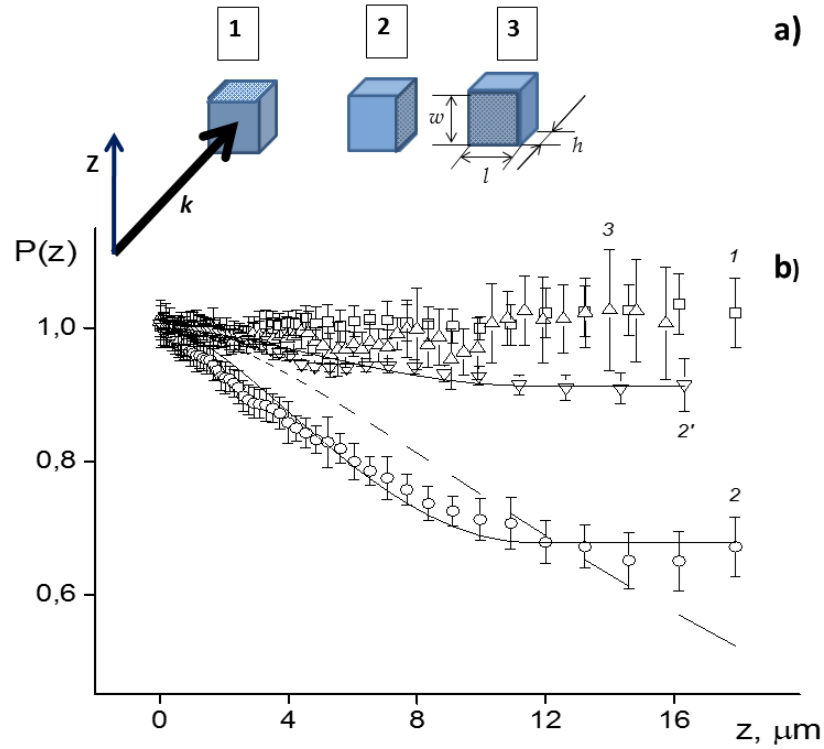
Fig. 2. The relative orientations of a block of hydrogel with dimensions $l \times w \times h$ and the BC growth surface ($l \times w$) in the neutron beam with respect to axes of SESANS setup, z and k (**a**): $z \perp (l \times w)$ *(1)*, $(z \times k) \parallel (l \times w)$ *(2)*, $(z \times k) \perp (l \times w)$ *(3)*. The ($l \times w$) surface is highlighted by a color pattern. The dependences of the reduced polarization, $P(z)$, on the spin-echo length, z, (**b**) for three HG2Tb orientations (1–3) and the second orientation of HG1Tb (2') are given. Solid lines present the results of fitting the experimental data using the formulas (9, 10). The dashed line corresponds to the best fit of the neutron refraction data with the formula.

350

355
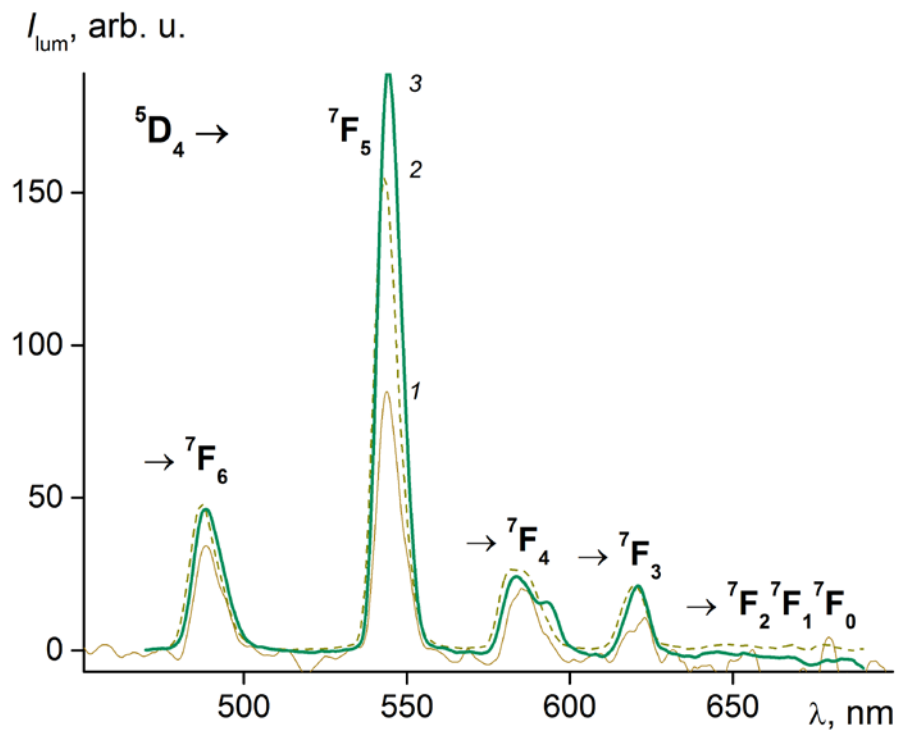
(a)
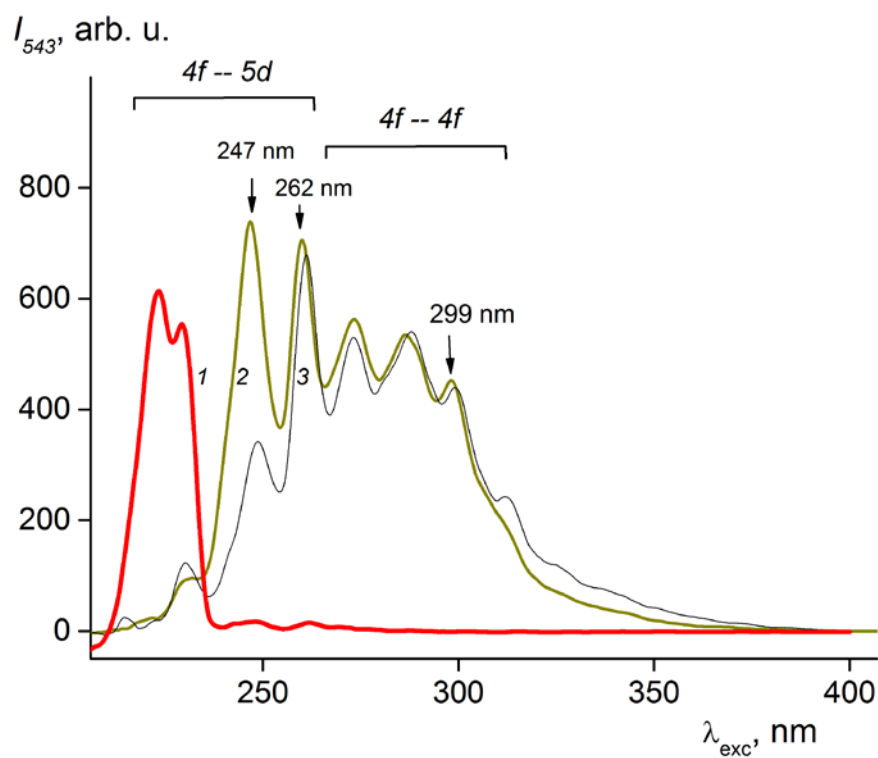
(b)

Fig. 3. Photoluminescence emission (*a*) and excitation (*b*) spectra for 0.536 mM Tb^{3+} in D_2O (*1*), HG1Tb (*2*), and air-dried HG1Tb composite (*3*). Luminescence excitation was at 299 nm (*a*). Luminescence was observed at 543 nm (*b*).

To verify the validity of assumptions about selective sorption, this mechanism was investigated by fluorescent methods. Besides, the inhomogeneities inside polymeric gels can be revealed on a molecular scale using lanthanide ions (Ln^{3+}) [25a]. Fig. 3 compares the excitation and emission spectra of Tb^{3+} in D_2O, of the luminescence hydrogel exposed to $TbCl_3$ solution in D_2O until equilibrium swelling was reached, and of the luminescence air-dried composite. The luminescence spectrum of HG1Tb (Fig. 3a) has a quasi-lined structure with characteristic peaks in the luminescence band at 490, 543, 580, 620 nm etc., which can be compared with the atomic resonance transitions in the luminescence spectra of Tb^{3+}, corresponding to the spectral lines $^5D_4 - {}^7F_J$, where J = 6—0 [25b].

In the luminescence excitation spectrum for HG1Tb (Fig. 3b, curve 2), peaks at 247 and 262 nm corresponding to *4f—5d*-transitions are present, and the peaks at 273, 286, 299, and 320 nm are attributed to *4f—4f* transitions [27]. For $TbCl_3$ solution in "heavy" water, these intense contributions at the above wavelengths were not observed (curve *1*). If HG1Tb was dried on air, the contribution of long wavelength part of excitation spectrum increase (compare curve *2* and *3*). These facts hold the idea that Tb^{3+} ions are adsorbed on BC microfibrils. Moreover, according to the authors [25a], polymeric gels could absorb more Ln^{3+} than is necessary to neutralize the network charges, i.e. negative ζ-potential of cellulose microfibrils. In our case, the impossibility could be expected to adopt a conformation of the microfibrils for Tb^{3+} in in which all positive charges are neutralized. Moreover, this factor may also lead to increase the Tb^{3+} concentration around the BC microfibrils forming the rigid scaffold in composite hydrogels.

The resulting increase in the efficiency of luminescence excitation for HG1Tb and HG2Tb may be because Tb^{3+} ions provide their virtual *5d* and *4f* atomic orbitals for lone electron pairs of the hydroxyl oxygen atoms of a matrix instead of water. Thus, it is possible to form a donor-acceptor coordination bond between Tb^{3+} ions and the matrix of the hydrogel. It is important that the bound organic compounds located near the central atom of the complex can absorb with a larger extinction coefficient in the range of 280—310 nm than lanthanide ions themselves [26]. Then, due to the resonant dipole–dipole interaction, electronic excitation energy is transferred from the "antenna" of the organic matrix to an isoenergetic level of Tb atom according to the Förster resonance mechanism (FRET). It can be concluded that Tb^{3+} ions are adsorbed by the hydrogel matrix; i.e., we are talking about a possible mechanism of selective sorption of Tb^{3+} ions on cellulose microfibrils.

The data obtained (by SESANS, luminescence) shows that it is impossible to account formally for the volume fraction (portion) of water in a biphasic approximation. After all, the values of φ_k in HG2Tb and HG2Tb(sel) are practically the same (Table 2). However, the value $P(z)$ for the second orientation decreases depending on the concentration of Tb^{3+}. The conclusion might be made that the water in the complex in the form of aqua ligands, the bound water, and the water just in the lacunas may produce different contributions when calculating the contrast [28]. Moreover, the authors [29, 30] showed by X-ray and neutron scattering that a first hydration shell could have a significantly higher density than that of the bulk solvent surrounding proteins in solution. They consider that it may be a general property of aqueous interfaces, what should be taken into account too in our case.

Strong uniaxial anisotropy is described by the model of oriented cylinders. It can be explained by the presence of "tunnels" (hollow cylinders) in the sample

with walls formed from compacted bacterial cellulose; these tunnels are filled with PAAm. The main volume of the sample outside the channels is also filled with PAAm.

Fig. 2b (curves *2* and *2'* for HG2Tb and HG1Tb, respectively) presents the results of fitting the experimental data with the use of Eq. (12).

Fitting yielded the following parameters: $D = (11.5\pm0.5)$ µm, $\varphi = 0.05\pm0.01$ for both samples; the contrast ($\Delta\rho_0$) for the HG1Tb sample is 0.3×10^{14} m^{-2}, and for the HG2Tb, the value was 0.49×10^{14} m^{-2}. The value of D does not depend on the above assumption about selective sorption.

Using the concept of curved tubes, one can assume that the channels are oriented perpendicularly to the BC growth surface, and their length substantially exceeds 20 µm (the maximum size currently available in the SESANS method). Under these conditions, it is easy to see that in the sample orientation 1, the experimental signal should be absent according to Eq. (10), since $L\rightarrow\infty$. For ideally oriented cylinders, the signal from the sample in orientation 3 should be observed as well as in the case of direction 2 (see Fig. 2a). However, the signal in orientation 3 was not observed. The question arise how it could be explained. The presence of a change in polarization in the SESANS data in only one orientation of the sample can be explained by large lengths of tubes. With the orientation of the tubes along spin-echo length direction no signal can be observed, which indicates that the length of the tubes is far above maximal spin-echo length (20 µm). With the orientation of the tubes parallel to the neutron beam, no change in polarization is observed. This is in agreement with the calculations by de Haan and co-authors [31], that standard scattering theories do not apply to scattering inhomogeneities of the sizes above 50 µm along the neutron beam, when using a wavelength of 2 Å. According to the examples given in his paper, the intensity will be much lower than in the usual Born's approximation. Therefore, the only signal that is measured is when the tubes are perpendicular to the neutron beam and the spin-echo length direction. Then the relevant length scale is the diameter of the tubes, which is in the micron range, where SESANS is sensitive, and the Born's approximation works.

Another possible reason that we obtained a SESANS signal in only one orientation of the sample is neutron refraction. In this case, we should observe a signal in only one orientation of the sample, i.e. with the cylinders perpendicular to both the spin echo length and neuron beam axes. The dashed line in Fig. 1b represents the best fit obtained for curve 2 with assuming neutron refraction. As can be seen, this fit does not describe the obtained signal. Therefore, none of the models used seem to describe the obtained data completely, but we assume that neutron refraction might cause an increase of the SESANS signal for oriented cylinders in orientation 2, which might lead to observed results.

Thus, the only registered signal in orientation 2 can be described by the correlation function of a cylinder with the long side oriented along the y-axis, and the observed dependence suggests that the diameter of the cylinder lies in the range of 11.5±0.5 µm.

Cryo-SEM data

We try to find some evidence of mesostructure anisotropy of BC and BC-PAAm hydrogels by using the cryo-SEM technique, which allows studying water swollen soft materials maintaining the sample as close as possible to its natural state. Samples can be observed while avoiding shrinkage or distortion that can occur with other sample preparation methods [32].

12

As it was mentioned early (section "Materials and methods") we obtain the cryo-SEM images (Fig. 4 and 5) for the samples fractured thru the plane mainly perpendicular to the surface of growth of matrix BC. Cryo-scanning electron micrographs of BC (Fig. 4) illustrate the significant features of its morphology that may have an impact on the composite hydrogels structure and properties. In the network structure, there are cavities (note spots 1 in Fig. 4a) with a size more than 10 µm that can be exits of "tunnels" formed by bacteria during biosynthesis. According to Thompson et al. [13] these tunnels are the result of bacteria motion while the BC pellicle grows starting from the air–liquid surface. The orientation of these tunnels is not traced rather accurately: they can be bent in various directions. However, in the right part of Fig. 4a, the rather extended vertical tunnel with a width from 20 to 50 µm is visible (spots 2).
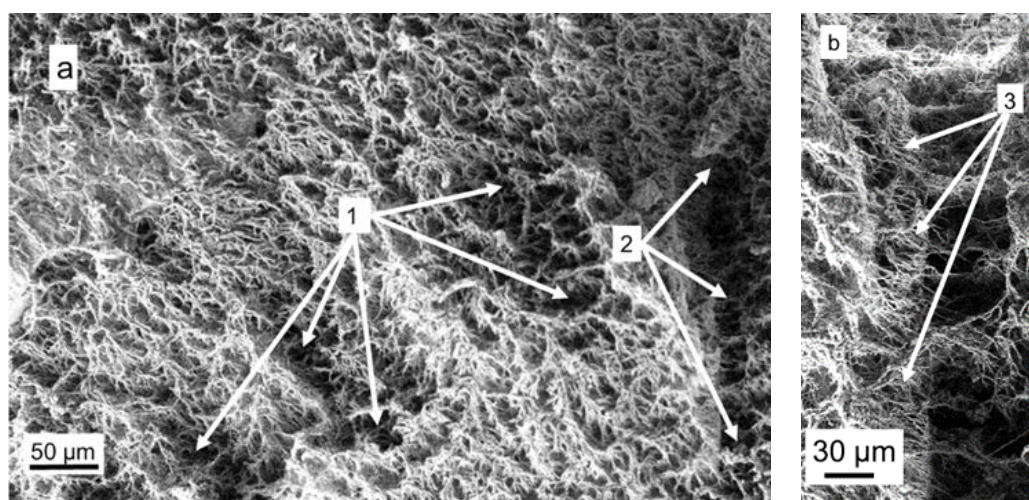

Fig. 4. Cryo-scanning electron micrographs of bacterial cellulose containing approx. 99 wt. % of water with different magnification: a – 500x, b – 2000x.

At bigger magnification (2000x) it is visible that "walls" of the tunnel are condensed with the congestion of the micro-fibrillar BC ribbons (spots 3 in Fig. 4b). This observation demands, of course, more careful studying. However, it correlates with SEM data for composite BC-PAAm hydrogels presented on Fig. 5: One can see the system of elliptic areas with a size from 10 to 50 µm (spots 1), which in our opinion are similar to the exits of vertically focused tunnels filled with polyacrylamide (Fig 5a). The two inhomogeneities rather extended, which can be the «walls» of such tunnels (with a size of about 20 µm), and condensed of cellulose chains, can be seen in Fig. 5b (spots 2). Speaking of "the condensed walls" of tunnels, we mean those, which are traced in Fig. 4b along the border of a "tunnel" for a frozen BC sample (spots 3).

According to [32] cryo-SEM methods are ideally suited to image hydrogels because the severe collapse and flattening due to dehydration does not exist in properly frozen specimens. Moreover, in the analysis of SEM data of composite hydrogels, it is necessary to consider that they contain a big amount of polyacrylamide, which substantially shields the physical grid formed by cellulose micro-fibrillar ribbons. At the same time, taken into account the various rigidity of cellulose and polyacrylamide, there is a high probability that at fractionation *(means "at production" of the chips)* of frozen BC-PAAm samples the destruction will happen on the polymer phases boundary, and it allows to observe the tunnel-like structural areas (Fig. 5c and d).

At still higher magnification (20 000x or 40 000x – Fig 5c and d, respectively) it is clear that there are domains with a size of *ca*. 1 micron in the IPN structure.

13

Even smaller regions with a dimension of tens nanometers are noticeable in domains of the micron size. The fractal structure seems to be ascertained on these SEM images. The objective of this study was not to examine the superfine structure. However, it is of some interest for the development of work with, in particular, the SANS data, which allows one to identify and analyze inhomogeneities with the size from tens until hundreds of nanometers for polymeric gels [33].
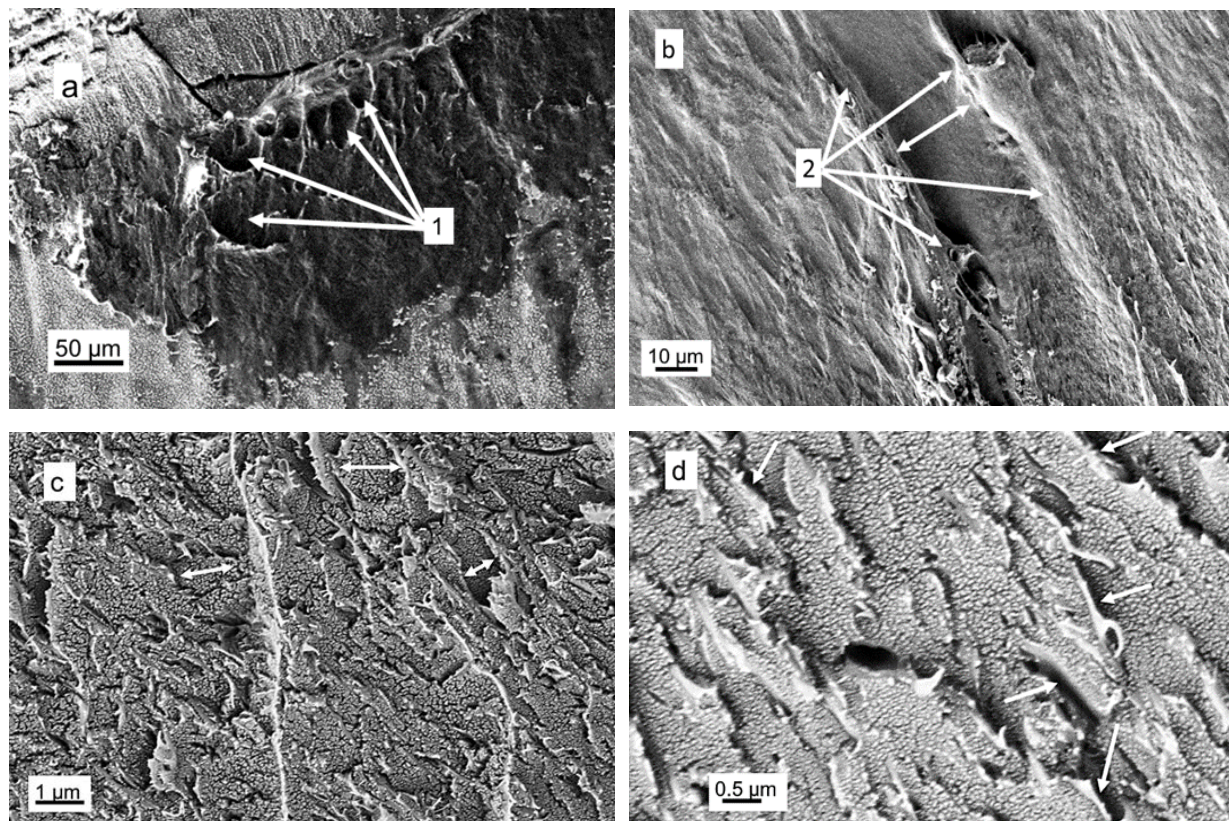

Fig. 5. Cryo-scanning electron micrographs of composite BC-PAAm hydrogel containing approx. 70 wt. % of water with different magnification: a – 500x, b – 2000x, c – 20 000x, d – 40 000x.

For the analysis of SESANS data, it is essential that between domains the interface designated in some spots by the arrows is determined (Fig. 5d). It is apparent that this border arises owing to the well-known effect of microphase separation between the polymeric IPN components [8]; for the system under investigation, it is possible to expect the emergence of an interface between macromolecules of PAAm and cellulose. Then on this interface, the diffusion of Tb^{3+} ions into a hydrogel will proceed above all. Thus, along an interface of polymeric phases, the concentration of the Tb^{3+} bound to the polymeric matrix is on the one – two orders higher than the average in the volume of a hydrogel, as leading to the strengthening of contrast between phases. We assume that the sorption of Tb^{3+} might preferably occur on cellulose chains. As can be seen in Fig. 4b, along the walls of the tunnels, the concentration of the cellulose chains is much higher than the average in the volume of a hydrogel. Accordingly, along the walls of the tunnels, the Tb^{3+} will concentrate and enhance the contrast between the BC and PAAm.

Conclusions

1. According to the SESANS study, the BC—PAAm hydrogels under investigation have been proven to possess a uniaxial anisotropy of micron structure with a characteristic size of 11.5±5 μm, the axis being normal to the BC growth surface. The contrast of the inhomogeneities of the structure manifested itself when $TbCl_3$ salt was added to the solvent.

2. The excitation spectra have revealed the intensive photoluminescence of hydrogels containing Tb^{3+} ions in the region from 280 until 310 nm. It indicates that these ions from solution are associated with the hydrogel matrix.

3. Thus, the results obtained by SESANS confirmed the assumption made in [11] that the anisotropy of the mechanical properties of these systems is caused by the specific structure of the BC matrix in the hydrogels, which according to Thompson et al. [13] has the oriented tunnel-like organization. This conclusion correlates with data of direct supervision of vertically focused heterogeneities by the cryo-SEM method. The more exact correlation of both methods requires further work in respect of studying of BC-PAAm hydrogels structure with a differing ratio of polymeric components of the interpenetrating polymeric network (BC and PAAm).

Acknowledgments

Appendix A. Supplementary data

Analytical dependence of the reduced polarization on the spin-echo length is described by the following equation [15]:

$$P(z) = \frac{P_{sample}(z)}{P_{solvent}(z)} = e^{\Sigma_t(G(z)-1)}, \tag{3}$$

$$\Sigma_t = t\lambda^2(\Delta\rho)^2\varphi(1-\varphi)\xi, \tag{4}$$

where z is the spin-echo length (varied in the SESANS experiments);
t is the thickness of the sample;
Σ_t is the average number of scattering events of the neutron in the sample;
$G(z)$ is the projection of the pair correlation function on the axis codirectional with z;
φ is the volume fraction of any of the phases in the two-phase system;
ξ is the correlation length of the scattering inhomogeneities;
λ is the neutron wavelength.

The dependence of $G(z)$ is a projection of the spatial correlation function $\gamma(r)$ on the quantization axis, along which correlations are measured in SESANS (spin-echo length, z):

$$G(z) = \int_z^{+\infty} \frac{\gamma(r)}{\sqrt{r^2 - z^2}} dr, \tag{5}$$

where the spatial correlation function γ(r) is defined as

$$\gamma(r) = \int_V \rho(r)\rho(r + r')dr', \tag{6}$$

where the integration is performed over the volume V of the system using the radius vector $r = (x, y, z)$ and $r' = (x', y', z')$.

From the experimental point of view, the $G(z)$ function is retrieved by

$$G(z) = \frac{lnP(z)}{lnP(\infty)}, \tag{7}$$

where P(z) is the polarization of the neutron beam, which passed through the sample and normalized to the polarization after passing through the cuvettes with solvent. The $P(\infty)$ value characterizes the fraction of the neutrons that are not scattered during transmission through the sample. Moreover, the value of the saturation level also provides information about the concentration by taking φ into account, information about the microstructure via ξ, and about the chemical structure through $\Delta\rho$ [15]:

$$P(\infty) \equiv e^{-\Sigma_t}. \tag{8}$$

As was mentioned before, due to strong anisotropy of the mechanical characteristics of the samples under investigation, it was expected to observe an orientation-dependent SESANS signal. Therefore, each sample was measured in three orthogonal orientations, schematically represented in Fig. 2a. In case of an anisotropic sample structure, it is likely to observe different SESANS signals for different sample orientations relatively to the setup geometry [19]. ~~In the present work, two different ideas were considered to describe the obtained experimental results: a scattering model of oriented cylinders and neutron refraction [20].~~ In the present work, the scattering model of oriented cylinders is considered to describe the obtained experimental results [20].

In case of oriented cylinders we will consider cylinders oriented along three different axes of Cartesian coordinates (x, y, z), connected with experimental setup. The x-axis corresponds to the neutron beam direction; the z-axis is the vertical axis along which the spin-echo length is being varied in the experiment; the y-axis is perpendicular to the former two and it should be noted that SESANS is insensitive to inhomogeneities in the y-direction. A detailed derivation of $G(z)$ functions for all cylinder orientations might be found in [14], here we will only show the $G(z)$ functions and corresponding correlation lengths expressions. As a starting point, we shall consider the autocorrelation function of a disc in 2 dimensions:

$$\gamma_c(r) = \begin{cases} \frac{2}{\pi}\left(cos^{-1}\left(\frac{r}{D}\right) - r\frac{\sqrt{D^2 - r^2}}{D^2}\right) if r \leq D. \\ 0, otherwise \end{cases} \tag{9}$$

For a cylinder with the long side coaxial with the z-axis of the setup and the cross section in the xy-plane we will have:

$$G(z) = 1 - z/L. \tag{10}$$

By integrating the former function over the diameter D, we will get the correlation length:

$$\xi = 2\int_0^D \gamma_c(x)dx = \frac{8D}{3\pi}, \tag{11}$$

which is the average length of all chords drawn inside a disk of diameter D.
Having the side of the cylinder parallel to y and its diameter in the xz-plane yields, for $z < D$:

$$G(z) = \int_0^D \gamma_c\left(\sqrt{x^2 + z^2}\right)dx, \tag{12}$$

and again the correlation length is $\xi = 8D/3\pi$.

16

If the cylinder is oriented with its side along x and its face in the zy-plane, the projection along x becomes, for $z < D$:

$$G(z) = \gamma_c(z) \qquad (13)$$

and the correlation length is in this case L:

$$\xi = 2 \int_0^D \left(1 - \frac{x}{L}\right) dx = L. \qquad (14)$$

~~In case of neutron refraction, the polarization of the neutron beam exponentially depends on the number of refractive elements on the beam pathway:~~

$$~~P(z) = (2\Delta\rho\lambda z \cdot K_1(2\Delta\rho\lambda z))^n; \qquad (15)~~$$

~~where $K_1(x)$ is the first-order modified Bessel function of the second kind. In case of oriented cylinder-like refractive elements, we can expect this effect only in the orientation of cylinders perpendicular to both spin-echo length and beam axes.~~

References

[1] Sciaretta FV. 5 to 8 years follow-up of knee chondral defects treated by PVA-H hydrogel implants. Europ Revi Medical Pharmacol Sci 2013;17:3031–38.

[2] Ku DN. New soft tissue implants using organic elastomers. Fred A, Filipe J, Gamboa H, editors. Biomedical engineering systems and technologies. Berlin: Springer-Verlag; 2008. pp. 85–95.

[3] (a) Gonzales JS, Alvarez VA. Mechanical properties of polyvinylalcohol/hydroxyapatite cryogel as potential artificial cartilage. J Mech Behav Biomed Mater 2014;34:47–56;
(b) Batista NA, Rodrigues AA, Bavaresco VP, Mariolani JRL, Belangero WD. Polyvinyl alcohol hydrogel irradiated and acetalized for osteochondral defect repair: mechanical, chemical, and histological evaluation after implantation in rat knees. Int J of Biomaterials 2012;582685:9 pages. http://dx.doi.org/10.1155/2012/582685.

[4] (a) Philippova OE. Responsive polymer gels. Polymer Science C 2000;42:208–228;
(b) Kuksenok O, Deb D, Yong X, Balazs AC. Designing biomimetic reactive polymer gels. Materials Today 2014;17:486–493. http://dx.doi.org/10.1016/j.mattod.2014.06.003;
(c) Ionov L. Hydrogel-based actuators: possibilities and limitations. Materials Today 2014;17:494–503. http://dx.doi.org/10.1016/j.mattod.2014.07.002.

[5] (a) Nandgaonkar AG, Krause WE, Lucia LA: Fabrication of cellulosic composite scaffolds for cartilage tissue engineering. Liu H, editor. Nanocomposites for musculoskeletal tissue regeneration. Amsterdam: Woodhead Publishing, Elsevier; 2016. pp. 187–212.
(b) Figueiredo ARP, Vilela C, Neto CP, Silvestre AJD, Freire CSR: Bacterial cellulose-based nanocomposites: roadmap for innovative materials. Thakur VK, editor. Nanocellulose polymer nanocomposites: fundamentals and applications. Hoboken, NJ, USA: John Wiley & Sons, Inc; 2015. pp. 17–64. [chapter 2.] doi: 10.1002/9781118872246.ch2

(c) Figueiredo Andrea GPR, Figueiredo ARP, Alonso-Varona A, Fernandes SCM, Palomares T, Rubio-Azpeitia E, Barros-Timmons A, Silvestre AJD, Neto CP, Freire CSR. Biocompatible bacterial cellulose-poly(2-hydroxyethyl methacrylate) nanocomposite films. BioMed Research International 2013;698141:1–14. http://dx.doi.org/10.1155/2013/698141

[6] (a) Ullah H, Santos HA, Khan T. Applications of bacterial cellulose in food, cosmetics and drug delivery. Cellulose 2016;23:22912314. DOI 10.1007/s10570-016-0986-y;
(b) Lin N., Dufresne A. Nanocellulose in biomedicine: Current status and future prospect. European Polymer Journal 2014;59:302–325.

[7] Astley OM, Chanliaud E, Donald AM, Gidley MJ. Structure of *Acetobacter* cellulose composites in the hydrated state. Int J Biol Macromol 2001;29:193–202.

[8] Sperling LH. Interpenetrating polymer network: an overview. Chapter 1. Klempner D, Sperling LH, Utracki LA, editors. Interpenetrating polymer networks. American Chemical Society, Advances in Chemistry; Washington, DC: American Chemical Society 1994;239:3–38. DOI: 10.1021/ba-1994-0239.ch001.

[9] Buyanov AL, Revel'skaya LG, Kuznetzov YuP, Shestakova AS. Cellulose-poly(acrylamide or acrylic acid) interpenetrating polymer membranes for the pervaporation of water-ethanol mixtures. J Appl Polym Sci 1998;69:761–768.

[10] Buyanov AL, Revel'skaya LG, Kuznetzov YuP, Khripunov AK. Cellulose-poly(acrylamide or acrylic acid) interpenetrating polymer membranes for the pervaporation of water/ethanol mixtures. II. Effect of ionic group content and cellulose matrix modification. J Appl Polym Sci 2001;80:1452–1460.

[11] Buyanov AL, Gofman IV, Revel'skaya LG, Khripunov AK, Tkachenko AA. Anisotropic swelling and mechanical behavior of composite bacterial cellulose (polyacrylamide or polyacrylamide-sodium polyacrylate) hydrogels. J Mech Behav Biomed Mater 2010;3:102–111.

[12] Buyanov AL, Gofman IV, Khripunov AK, Tkachenko AA, Ushakova EE. High-strength biocompatible hydrogels based on poly(acrylamide) and cellulose: synthesis, mechanical properties and perspectives for use as artificial cartilage. Polymer Sci A 2013;55:302–312.

[13] Thompson NS, Carlson JA, Kaustinen YM, Uhlin KI. Tunnel structures in *Acetobacter xylinum*. Int J Biol Macromol 1988;10:126–127.

[14] (a) Martínez-Sanz M, Gidley MJ, Gilbert EP. Application of X-ray and neutron small angle scattering techniques to study the hierarchical structure of plant cell walls: A review. Carbohydrate Polymers 2015;125:120–134. DOI: 10.1039/C5SM02085A;
(b) Velichko EV, Buyanov AL, Chetverikov YuO, Duif CP, Bouwman WG, Smyslov R.Yu. Mesostructure anisotropy of bacterial cellulose-polyacrylamide

hydrogels as studied by spin-echo small-angle neutron scattering. arXiv:1608.00544 [physics.chem-ph].
(c) Håkansson K. M. O., Fall A. B., Lundell F., Yu S., Krywka C., Roth S. V., Santoro G., Kvick M., Wittberg L. P., Wågberg L., Söderberg L. D. Hydrodynamic alignment and assembly of nanofibrils resulting in strong cellulose filaments. Nature Communications 2014;5:4018.

[15] Andersson R, van Heijkamp LF, de Schepper IM, Bouwman WG. Analysis of spin-echo small-angle neutron scattering measurements. J Appl Cryst 2008;41:868–885.

[16] (a) Evmenenko G, Budtova T, Buyanov A, Frenkel S. Structure of polyelectrolyte hydrogels studied by SANS. Polymer 1996;37:5499–5502.
(b) Evmenenko G, Alexeev V, Budtova T, Buyanov A, Frenkel S. Swelling-induced structure changes of polyelectrolyte gels. Polymer 1999;40:2975–2979.

[17] Rekveldt MT, Plomp J, Bouwman WG, Kraan WH, Grigoriev SV, Blaauw M. Spin-echo small angle neutron scattering in Delft. Rev Sci Instrum 2005;033901(76): 9 pages.

[18] Uca O, Bouwman WG, Rekveldt MT. Model calculations for the spin-echo small-angle neutron-scattering correlation function. J Appl Cryst 2003;36:109–116.

[19] Andersson R., Bouwman W. G., Plomp J., Mulder F. M., Schimmel H. G., de Schepper M. Structure, anisotropy and fractals in compressed cohesive powders. Powder Technol 2009;189:6–13.

[20] Buyanov AL, Gofman IV, Bozhkova SA, Saprykina NN, Kochish AYu, Netyl'ko GI, Khripunov AK, Smyslov RYu, Afanas'ev AV, Panarin EF Composite Hydrogels Based on Polyacrylamide and Cellulose: Synthesis and Functional Properties. Rus J of Appl Chemistry 2016;89:772−779.

[21] Öztürk HB, Vu-Manh H, Bechtold T. Interaction of cellulose with alkali metal ions and complexed heavy metals. LenzingerBerichte 2009;87:142–150.

[22] Norkus E, Vaiciuniene J, Virbalyte D. Interaction of copper (II) with cellulose pulp. Chemija (Vilnus) 2002;13:75–84.

[23] Fink HP, Purz HJ, Bohn A, Kunze J. Investigation of the supramolecular structure of never dried bacterial cellulose. Macromol Symp 1997;120:207–217.

[24] (a) K. Kanamaru, Wasseraufnahme in ihrer Beziehung zur zeitlichen Erniedrigung des Z-Potentials von Fasernin Wasser. Kolloid Z. 168 (1960) 115 DOI: 10.1007/BF01507420.
(b) Kreze T., Stana-Kleinschek K., Ribitsch V. The sorption behaviour of cellulose fibres. Lenzinger Berichte. 2001; 80: 28—33.

[25] (a) Smirnov V. A., Philippova O. E., Sukhadolski G. A., Khokhlov A. R. Multiplets in Polymer Gels. Rare Earth Metal Ions Luminescence Study. Macromolecules 1998, 31, 1162-1167.
(b) Bünzli JC. On the design of highly luminescent lanthanide complexes. Coordination Chemistry Reviews 2014; 293—294.

[26] (a) Ballauf M., Jusufi A. Anomalous small-angle X-ray scattering: analyzing correlations and fluctuations in polyelectrolytes. Colloid Polym Sci 2006; 284: 1303—1311. DOI 10.1007/s00396-006-1516-5
(b) Manning G. S. Limiting Laws and Counterion Condensation in Polyelectrolyte Solutions. III. An Analysis Based on the Mayer Ionic Solution Theory. J Chem Phys 1969;51:3249. http://dx.doi.org/10.1063/1.1672502
(c) Mei Y., Lauterbach K., Hoffmann M., Borisov O. V., Ballauff M., Jusufi A. Collapse of Spherical Polyelectrolyte Brushes in the Presence of Multivalent Counterions. PRL 97, 158301 (2006).
(d) Borisov O. V., Zhulina E. B., Leermakers F. A.M., Ballauff M., Müller A.H.E. Conformations and Solution Properties of Star-Branched Polyelectrolytes. Adv Polym Sci (2011) 241: 1–55. DOI:10.1007/12_2010_104

[27] (a) Kumar JS, Pavani K, Sasikala T, Jayasimhadri M, Jang K, Moorthy LR. Concentration dependent luminescence characteristics of $^5D_4$ and $^5D_3$ excited states of Tb^{3+} ions in CFB glasses, Oxide-based materials and devices II. Teherani FH, Look DC, Rogers DJ, editors. Proc. SPIE 7940, 79401H.
(b) Ebendor-Heidepriem H, Ehrt D. Formation and UV absorption of cerium, europium and terbium ions in different valencies in glasses. Optical Materials 2000;15:7—25.
(c) Rosendo A., Flores M., Co´rdoba G., Rodrı´guez R., Arroyo R. Synthesis, characterization and luminescence properties of Tb^{3+} and Eu^{3+}-doped poly(acrylic acid). Materials Letters 57 (2003) 2885– 2893.

[28] Rajapaksha A, Stanley CB, Todd BA. Effects of macromolecular crowding on the structure of a protein complex: a small-angle scattering study of superoxide dismutase. Biophysical J 2015;108:967–974.

[29] Svergun DI, Richard S, Koch MHJ, Sayers Z, Kuprin S, Zaccai G. Protein hydration in solution: experimental observation by x-ray and neutron scattering. Proc. Natl. Acad. Sci. USA 1998;95:2267–2272.

[30] Timasheff SN. Protein hydration, thermodynamic binding, and preferential hydration. Biochem 2002;41:13473–13482.

[31] Haan, V. de, Plomp, J., Bouwman, W.G., Trinker M., Rekveldt M. T., Duif C. P., Jericha E., Rauch H., and Well A. A. van. Phase-object approximation in small-angle neutron scattering experiments on silicon gratings. J Appl Cryst 2007;40:151—157. DOI: 10.1107/S0021889806047558

[32] Apkarian RP, Wright ER. Cryo-and-cryo-etch methods for quality preservation of hydrogels imaged at high magnification by low temperature SEM. MicroscMicroanal 11(Suppl 2); 2005. DOI: 10.1017/S1431927605500163.

770   [33] Zaroslov Yu. D., Gordeliy V. I., Kuklin A. I., Islamov A. H., Philippova O. E., Khokhlov A. R., and Wegner G. Self-Assembly of Polyelectrolyte Rods in Polymer Gel and in Solution: Small-Angle Neutron Scattering Study. Macromolecules 2002, 35, 4466-4471.